

## MIT Open Access Articles

*M13 Virus#Based Framework for High Fluorescence Enhancement*

The MIT Faculty has made this article openly available. **Please share** how this access benefits you. Your story matters.

**Citation:** Huang, Shengnan et al. "M13 Virus#Based Framework for High Fluorescence Enhancement." *Small* 15, 28 (May 2019): 1901233 © 2019 WILEY#VCH Verlag GmbH & Co

**As Published:** <http://dx.doi.org/10.1002/sml.201901233>

**Publisher:** Wiley

**Persistent URL:** <https://hdl.handle.net/1721.1/125906>

**Version:** Author's final manuscript: final author's manuscript post peer review, without publisher's formatting or copy editing

**Terms of use:** Creative Commons Attribution-Noncommercial-Share Alike



### **M13 Virus-based Framework for High Fluorescence Enhancement**

*Shengnan Huang, Jifa Qi, Dane W. deQuilettes, Mantao Huang, Ching-Wei Lin, Neelkanth M. Bardhan, Xiangnan Dang, Vladimir Bulović, Angela M. Belcher\**

S. Huang, M. Huang, Prof. A.M. Belcher  
Department of Materials Science and Engineering, Massachusetts Institute of Technology,  
77 Massachusetts Avenue, Cambridge, Massachusetts 02139, USA  
E-mail: belcher@mit.edu

Dr. J.Qi, Prof. A.M. Belcher  
Department of Biological Engineering, Massachusetts Institute of Technology,  
77 Massachusetts Avenue, Cambridge, Massachusetts 02139, USA

Dr. D.W. deQuilettes, Prof. V. Bulović  
Organic and Nanostructured Electronics Laboratory, Massachusetts Institute of Technology,  
77 Massachusetts Avenue, Cambridge, Massachusetts 02139, USA

S. Huang, Dr. J. Qi, Dr. C-W Lin, Dr. N.M. Bardhan, Dr. X. Dang, Prof. A.M. Belcher  
The David H. Koch Institute for Integrative Cancer Research, Massachusetts Institute of  
Technology, 77 Massachusetts Avenue, Cambridge, Massachusetts 02139, USA

Keywords: fluorescence imaging, surface plasmon, fluorescence enhancement, M13 virus

Fluorescence imaging is a powerful tool for studying biologically relevant macromolecules, but its applicability is often limited by the fluorescent probe, which must demonstrate both high site-specificity and emission efficiency. In this regard, M13 virus, a versatile biological scaffold, has previously been used to both assemble fluorophores on its viral capsid with molecular precision and to also target a variety of cells. Although M13-fluorophore systems are highly selective, these complexes typically suffer from poor molecular detection limits due to low absorption cross-sections and moderate quantum yields. To overcome these challenges, we develop a co-assembly of the M13 virus, cyanine 3 dye, and silver nanoparticles to create a fluorescent tag capable of binding with molecular precision with high emissivity. Enhanced emission of cyanine 3 of up to 24-fold is achieved by varying nanoparticle size and particle-fluorophore separation. In addition, it is found that the fluorescence enhancement increases with increasing dye surface density on viral capsid. Finally, this highly fluorescent probe is applied for *in vitro* staining of *E. coli*. These results demonstrate an inexpensive framework for

achieving tuned fluorescence enhancements. The methodology developed in this work is potentially amendable to fluorescent detection of a wide range of M13/cell combinations.

Key words: fluorescence imaging, surface plasmon, fluorescence enhancement, M13 virus

Fluorescence imaging has been broadly applied in the field of bioimaging, as one is able to rapidly diagnose diseases at a relatively low cost.<sup>[1,2]</sup> However, its applicability is limited by the fluorescence moiety, which should demonstrate specific site binding efficiency and high fluorescence yield.<sup>[3]</sup> In this regard, M13 virus-fluorophore complex has been developed for fluorescence-based imaging.<sup>[4-6]</sup> M13 virus is a type of filamentous virus, which is approximately 880 nm in length and 6.5 nm in diameter. It is a versatile scaffold with five coat proteins (p3, p5, p7, p8, p9) that are able to display material specific peptides and/or targeting moieties with genetic engineering.<sup>[6-11]</sup> For example, using phage display, Yi *et al.* engineered the p8 major coat proteins for carbon nanotube (CNT) assembly and the p3 minor coat protein for prostate cancer targeting.<sup>[6]</sup> In addition, M13 virus has natural binding affinity towards bacteria that expresses F'-pili. Bardhan *et al.* used it to assemble CNT for *in vivo* imaging of bacterial infections.<sup>[5]</sup> Although M13-fluorophore systems are highly selective, these systems suffer from low molecular detection limit due to low quantum yields of fluorophores.<sup>[12]</sup>

One promising approach to improving molecular detection sensitivity of the M13-fluorophore complex is to introduce metal nanoparticles to the complex to enhance the fluorescence. The presence of metal nanoparticles near fluorophores enhances the fluorophore excitation rate via local electric field enhancement. In addition, it modifies the radiative decay rate, but can also open new nonradiative decay channels (dissipative), and hence modify the quantum yield and lifetime of fluorophores.<sup>[13,14]</sup> As the enhanced excitation rate (proportional to  $1/(\varepsilon(\omega_1) + 2)$ , where  $\varepsilon(\omega_1)$  is the frequency dependent dielectric constant of metal nanoparticle with  $\omega_1$  being the excitation frequency of the fluorophore) and radiative decay rate (proportional to  $1/(\varepsilon(\omega_2) + 2)$ , where  $\omega_2$  is the emission frequency of the fluorophore) and

the induced nonradiative decay rate (proportional to  $1/(\varepsilon(\omega_2) + 1)$ ) have different spectral dependence, it is demonstrated by both theoretical calculations and experiment measurements that maximum fluorescence enhancement occurs when the fluorophores emits to the red of the plasmon resonance peak of the nanoparticles (assuming  $\omega_1 = \omega_2$ ).<sup>[13–16]</sup> With silver nanoparticle (AgNP, plasmon resonance peak 400 nm), Bharadwaj *et al.* achieved 14-fold fluorescence enhancement of Alexa Fluor 488 (excitation wavelength 488 nm).<sup>[13]</sup> Anger *et al.* used gold nanoparticle (AuNP, plasmon resonance peak 520 nm) to enhance the emission of Nile blue (excitation wavelength 635 nm) and achieved an enhancement factor of 8-fold.<sup>[14]</sup> Furthermore, an optimal distance between the fluorophore and metal nanoparticle should be achieved for maximum fluorescence enhancement, as there is competition between nonradiative energy transferring from fluorophore to metal nanoparticle and excitation rate enhancement.<sup>[14,15]</sup> Conventional approaches for controlling the distance are to anchor fluorophores on the surface of nanoparticles wherein the surface of the metal nanoparticles are modified with a spacer.<sup>[17–19]</sup> For instance, Tovmachenko *et al.* used SiO<sub>2</sub> as spacer between AgNPs (diameter 47.2 nm) and Cascade Yellow and reported a fluorescence enhancement of 12.5-fold.<sup>[20]</sup> Zhang *et al.* used oligonucleotide as spacer between AgNP (diameter 20 nm) and Cy5 dye, and observed a 7-fold fluorescence enhancement, wherein the distance was controlled by the number of base pairs in the oligonucleotide.<sup>[21]</sup> In order to achieve high selectivity towards cells, the surface of metal nanoparticles is further modified with targeting ligands (antibodies, peptide etc.). However, this method has its limitations as excessive loading of ligands will reduce the targeting capabilities of the ligands and decrease the ability of metal nanoparticles to bind to finite number of receptors on cells.<sup>[9,22]</sup>

To achieve high detection specificity and high fluorescence load per cell receptor, we develop a fluorescent probe using M13 virus for the co-assembly of fluorophores and metal nanoparticles for the first time. Specifically, we use M13 virus as a biological template for the co-assembly of sulfo-Cy3 molecules (Cy3) and AgNPs. The M13 virus variant of E3 (–AEEE

inserted at the N-terminus of the major coat protein) was used in the study for its ease of amplification. Cy3 molecules are chemically conjugated to the exposed amines (-lysine residue and N-terminus) on the viral coat protein via EDC/NHS reaction.<sup>[23]</sup> Since distance between fluorophores and plasmonic nanoparticles are crucial for fluorescence enhancement, we add a spacer of polyethylene glycol (PEG) of various molecular weight (mol.wt.) between Cy3 molecules and AgNPs for optimum fluorescence enhancement.<sup>[24]</sup> The spacer we adopt in our study is hetero- PEG molecules namely, carboxyl-PEG-thiol (CTPEG). The carboxyl group of the CTPEG molecules is conjugated to the amine groups on the virus surface, and the exposed thiol groups act as anchoring sites for AgNPs.<sup>[21]</sup> The synthesis procedure of the nanocomplex is illustrated in **Scheme 1**, and the details can be found in the Supporting Information. With this design, we used a versatile biological scaffold for the co-assembly of Cy3 molecules and AgNPs; we studied the fluorescence emission properties of Cy3 molecules and achieved a 24-fold fluorescence enhancement. By combining fluorescence enhancement and the versatility of M13 virus, we applied this M13-based fluorescence probe for *in vitro* bacteria detection.

In this work, we used AgNPs to enhance the fluorescence of Cy3. As shown in **Figure 1**, AgNPs with diameter of 20/30/40 nm (orange/green/blue line) have plasmon peak of around 400 nm with a photon energy difference of less than 5%. The E3-Cy3 complex has major absorption peak of 550 nm (black line) and emission peak of 570 nm (red line), giving a small Stokes shift of around 20 nm. Hence, the emission of Cy3 is red-shifted to the plasmon resonance of AgNPs, thus promising strong fluorescence enhancement.<sup>[13–15]</sup> In addition, theoretical calculations show that AgNPs (with diameter larger than 20nm) are able to enhance the emission of E3-Cy3 when placed 5 nm from Cy3 via excitation rate enhancement and quantum yield enhancement (Figure S1). We also attempted to use AuNPs with plasmon resonance of 520nm (diameters 20/30/40 nm) for fluorescence enhancement of E3-Cy3 complex. This resulted in much smaller fluorescence enhancement compared to AgNPs (Figure S2), which is consistent with our theoretical calculations (Figure S1d-f).

In order to optimize the fluorophore emission enhancement enabled by metal nanoparticles in this study, we explore the effect of both fluorophore-metal nanoparticle distance and nanoparticle size. The distance is varied by modifying the E3 virus surface with CTPEG molecules and Cy3 molecules (E3-Cy3-CTPEG complex). The PEG chains act as spacers between Cy3 molecules and AgNPs, and the exposed thiol groups are anchoring points for AgNPs via the thiol-silver bonding (E3-Cy3-CTPEG-AgNP complex). **Figure 2** shows representative transmission electron microscopy (TEM) images of the AgNPs assembled along the CTPEG molecules modified E3 virus surface (please refer to Figure S3 for low magnification TEM images). In the E3-Cy3-CTPEG-AgNPs complex, AgNPs (diameters of 20/30/40 nm) assemble along the E3 virus surface forming chain-like structures, where the PEG chains act as a spacer between Cy3 dye and AgNPs. The absorption spectrum of E3-Cy3-CTPEG-AgNPs is shown in Figure S4. Due to the change of the local refractive index, there's slight red-shift (<5 nm) of the plasmon resonance peak of the AgNPs.

After forming the nano-complex, we then proceed to study the fluorescence enhancement. **Figure 3a** summarizes the results of fluorescence enhancement factors (EFs) when 1990 copies of Cy3 are conjugated to E3 surface (Table S2). By varying the mol. wt. of PEG chains and size of AgNPs, we are able to tune the fluorescence EF by changing Cy3-AgNP distance as illustrated in Figure S5. A maximum EF of ~ 24-fold is achieved for the 40 nm AgNPs when the mol. wt. of PEG is 2000g/mol. For the same PEG mol. wt., larger AgNPs tend to gain stronger fluorescence enhancement than smaller AgNPs, which is consistent with our theoretical calculations (Figure S6a). This could be partially ascribed to the higher local electric field in the vicinity of larger metal nanoparticles, which leads to stronger local field enhancement (Figure S6d-f) and higher excitation rate enhancement of fluorophores (Figure S6b).<sup>[25]</sup> In addition, the quantum yield enhancement also increases with increasing AgNP size (Figure S6c). For all the three AgNP sizes in this study, fluorescence EF increases and then decreases with the mol.wt. of PEG molecules. At small mol. wt. of 635 g/mol (Cy3-AgNP

distance of 2~3 nm as in Figure S5b), no fluorescence enhancement is observed for all of the three sizes. At short dye-metal nanoparticle distances, nonradiative energy transfer from dye molecules to metal nanoparticles leads to decreased quantum yield and quenching of fluorescence emission.<sup>[14,15]</sup> At PEG mol. wt. of 2000 g/mol, we have observed an EF of ~15-fold for the 30 nm AgNP. To better understand the fluorescence enhancement, we also conducted fluorescence lifetime measurements. Figure 3b shows a substantial lifetime reduction when placing AgNPs near Cy3 molecules. The fitted lifetime value after deconvolution of the IRF of the E3-Cy3-CTPEG2k complex without AgNPs (Figure 3b red triangle) is  $\tau = 680$  ps, which decreased to  $\tau = 58$  ps (Figure 3b green dot) upon placing AgNPs with diameter of 30 nm near the complex. We note that the lifetime of the complex with AgNPs appears to be limited by the instrument response function (IRF) of the setup (black squares in Figure 3b), and therefore may have an even faster decay rate than reported here. The combination of increased steady-state fluorescence intensity (Figure 3a) along with the faster decay upon inclusion of AgNPs (Figure 3b) is consistent with previous reports that the proximity of fluorophores to metal nanoparticles leads to an increased radiative decay rate and shortened lifetime.<sup>[17,21,26]</sup>

In conventional surface plasmon enhanced fluorescence structures, an ensemble of fluorophores are placed in adjacent to metal nanoparticle core with spacers in between them. With the neighboring distances among fluorophores shortened, energy transfer among fluorophores occurs;<sup>[27]</sup> this may influence surface plasmon enhanced fluorescence. However, to the best of our knowledge, there are no reports about the effect of fluorophore surface density on surface plasmon enhanced fluorescence. On the other hand, the versatility of M13 virus allows us to conjugate small fluorescent dye molecules with various surface densities. Hence, we then studied the surface density effect of dye molecules on surface plasmon enhanced fluorescence using M13 virus as template. We first conjugated CTPEG2k molecules to E3 virus surface to ensure the same spacer thickness. After that, we then conjugated approximately 400,

600, and 1200 copies of Cy3 molecules to E3 surface (Figure S7, Table S3). We first examined the surface density effect of Cy3 dye on the absorption spectrum of Cy3. As shown in **Figure 4a**, the intensity of the hypsochromic peak at around 512 nm increases with increasing surface grafting density of Cy3 on virus surface. This phenomenon of Cy3 dye is ascribed to increased interactions between adjacent dye molecules via  $\pi$ -orbital stacking, forming H-aggregates in solution.<sup>[28,29]</sup> We then sought to study how the increased interactions among neighboring Cy3 dyes change the quantum yield of the dye. By varying the optical densities at 532 nm (the excitation wavelength), we measured the fluorescence and the results are summarized in Figure 4b. As the slopes of the linear fits are proportional to the quantum yields,<sup>[30]</sup> we find that the quantum yield of Cy3 dye decreases with increasing surface density. After inclusion of AgNPs with diameter of 30 nm, we measured the surface plasmon enhanced fluorescence and the EF is summarized in Figure 4c. We find that the EF increases with increasing Cy3 surface density or decreasing dye quantum yield. A similar EF dependence on intrinsic quantum yield of fluorophores has been observed by Lakowicz *et al.*<sup>[31]</sup> In our design, the spacer thickness between Cy3 dyes and AgNPs is the same for all three dye surface densities, which means the local electric field enhancement and thereby the excitation rate enhancement is the same for the three cases. Hence, the difference in EF arises from the quantum yield modification by AgNPs. Upon inclusion of AgNPs to the M13-Cy3 complex, the enhanced radiative decay rate ( $\gamma_r$ ) and new non-radiative decay rate ( $\gamma_{rabs}$ ) are independent of the Cy3 surface density. They would bring the modified quantum yield ( $q$ ) of Cy3 close to the value of  $\frac{\gamma_r}{\gamma_r + \gamma_{rabs}}$ . This effect is more prominent when Cy3 has lower intrinsic quantum yield ( $q^0$ ) and higher surface density. In other words, AgNPs offer higher quantum yield enhancement ( $q/q^0$ ) and hence higher fluorescence enhancement (Figure S8) when Cy3 has higher surface density.

We have developed a highly bright fluorescent probes with surface plasmon enhanced fluorescence. In the subsequent section, we demonstrate that our highly emissive fluorescent



probe can be used for *in vitro* bacteria detection. Bardhan *et al.* have assembled CNT along the surface of M13 virus forming the M13-CNT complex and applied it to bind more specifically towards F'-positive bacteria compared to F'-negative bacteria both *in vitro* and *in vivo*.<sup>[5]</sup> In addition, assembling magnetic nanoparticles (MNP) along the surface of E3 virus with p3 expressing SPARC-binding peptide, Ghosh *et al.* have applied the M13-MNP complex for *in vivo* targeting of prostate cancer.<sup>[9]</sup> Hence, we are able to use the above fluorescent probe to target *E. coli* (ER2738, F'-positive) in this work. We stained the cell wall of *E. coli* with Alexa Fluor 647 dye (maximum absorption at 650 nm, emission peak at 665 nm). With this, we are able to evaluate whether the fluorescent signal of our fluorescent probes co-localizes with *E. coli*. The fluorescence signal of our fluorescent probes and Alexa Fluor 647 dye were captured with DeltaVision-OMX Super-Resolution Microscope with widefield illumination. **Figure 5a** shows a fluorescence image of E3-CTPEG2k-Cy3-AgNP30nm complex (green, excitation laser line 565 nm). Figure 5b shows the fluorescent image of *E. coli* stained with Alexa Fluor 647 (red) overlapped perfectly with the fluorescent images of E3-CTPEG2k-Cy3-AgNP30nm complex (green). More examples of fluorescent probes staining *E. coli* can be found in Figure S9. Hence, we are able to use our highly emissive plasmon enhanced fluorescent probes for *in vitro* bacteria detection. This opens great potential for applying M13 virus-based framework for a wide range of *in vivo* imaging and detection.

In conclusion, we have demonstrated surface plasmon enhanced fluorescence with an enhancement factor of up to 24-fold using the M13 virus-based framework. The distance between Cy3 and AgNPs was controlled by PEG molecules of different mol. wt.. When placing AgNPs near the virus surface assembled with Cy3, the emission intensity increases and fluorescence lifetime decreases, which can be attributed to an increase in the radiative emission rate. Exploiting the versatility of M13 virus, we coated the viral capsid with Cy3 of varying surface densities and studied the effect of dye surface density on surface plasmon enhanced

fluorescence. We find that increasing dye surface density leads to lower quantum yield and higher enhancement factor. This elucidates that in our study, AgNPs enhance more of the quantum yield when the intrinsic quantum yield of Cy3 is lower. Finally, we applied this M13-virus based framework as imaging probes for *in vitro* imaging of *E. coli*. In the future, phage display method that enables M13 virus to express specific targeting moiety would open great potential to apply this framework for *in vivo* imaging and detection.

### Acknowledgements

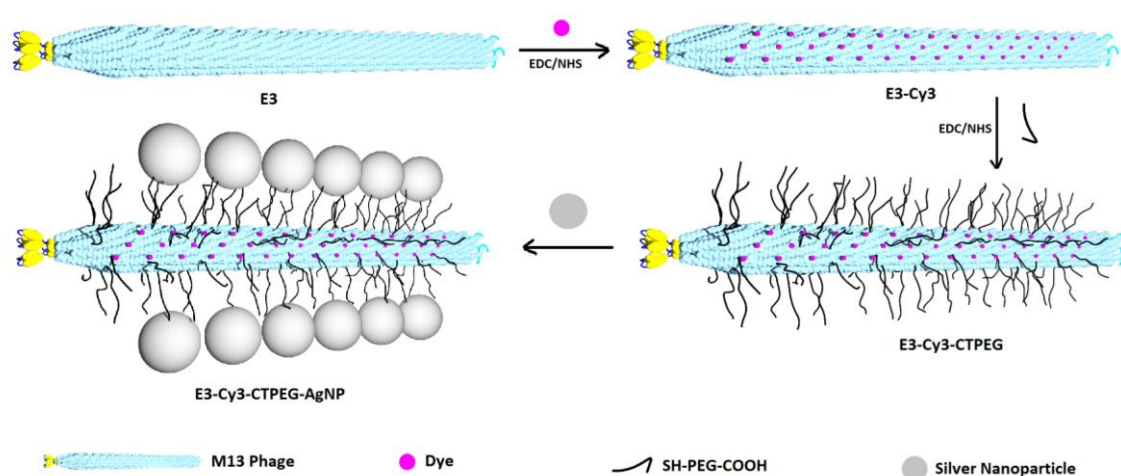
The authors appreciate the help of Dr. Eliza Vasile (Koch Institute for Integrative Cancer Research, MIT) for doing super-resolution microscope. This work was supported by the Marble Center for Cancer Nanomedicine and the U.S. Defense Advanced Research Projects Agency's Living Foundries program award HR0011-15-C-0084.

### References

- [1] R. Weissleder, M. J. Pittet, *Nature* **2008**, 452, 580.
- [2] X. Dang, L. Gu, J. Qi, S. Correa, G. Zhang, A. M. Belcher, P. T. Hammond, *Proc. Natl. Acad. Sci.* **2016**, 113, 5179.
- [3] D. A. Silbaugh, L. Ferrer-Tasies, J. Faraudo, J. Veciana, N. Ventosa, B. A. Korgel, *Langmuir* **2017**, 33, 14366.
- [4] D. Ghosh, A. F. Bagley, Y. J. Na, M. J. Birrer, S. N. Bhatia, A. M. Belcher, *Proc. Natl. Acad. Sci.* **2014**, 111, 13948.
- [5] N. M. Bardhan, D. Ghosh, A. M. Belcher, *Nat. Commun.* **2014**, 5, 1.
- [6] H. Yi, D. Ghosh, M. H. Ham, J. Qi, P. W. Barone, M. S. Strano, A. M. Belcher, *Nano Lett.* **2012**, 12, 1176.
- [7] S.-W. Lee, C. Mao, C. E. Flynn, A. M. Belcher, *Science* **2002**, 296, 892.
- [8] Y. J. Lee, H. Yi, W.-J. Kim, K. Kang, D. S. Yun, M. S. Strano, G. Ceder, A. M. Belcher, *Science* **2009**, 324, 1051.

- [9] D. Ghosh, Y. Lee, S. Thomas, A. G. Kohli, D. S. Yun, A. M. Belcher, K. A. Kelly, *Nat. Nanotechnol.* **2012**, 7, 677.
- [10] V. Puddu, C. C. Perry, *ACS Nano* **2012**, 6, 6356.
- [11] Y. Huang, C.-Y. Chiang, S. K. Lee, Y. Gao, E. L. Hu, J. De Yoreo, A. M. Belcher, *Nano Lett.* **2005**, 5, 1429.
- [12] A. Nish, J. Y. Hwang, J. Doig, R. J. Nicholas, *Nat. Nanotechnol.* **2007**, 2, 640.
- [13] P. Bharadwaj, L. Novotny, *Opt. Express* **2007**, 15, 14266.
- [14] P. Anger, P. Bharadwaj, L. Novotny, *Phys. Rev. Lett.* **2006**, 96, 3.
- [15] M. Thomas, J. J. Greffet, R. Carminati, J. R. Arias-Gonzalez, *Appl. Phys. Lett.* **2004**, 85, 3863.
- [16] Y. Chen, K. Munechika, D. S. Ginger, *Nano Lett.* **2007**, 7, 690.
- [17] K. Aslan, M. Wu, J. R. Lakowicz, C. D. Geddes, *J. Am. Chem. Soc.* **2007**, 1524.
- [18] F. Zhang, G. B. Braun, Y. Shi, Y. Zhang, X. Sun, N. O. Reich, D. Zhao, G. Stucky, *J. Am. Chem. Soc.* **2010**, 132, 2850.
- [19] Y. Zhai, L. Meng, L. Xu, L. Yuan, Z. Yang, J. Hu, X. Duan, *Plasmonics* **2017**, 12, 263.
- [20] O. G. Tovmachenko, C. Graf, D. J. Van Den Heuvel, A. Van Blaaderen, H. C. Gerritsen, *Adv. Mater.* **2006**, 18, 91.
- [21] J. Zhang, Y. Fu, M. H. Chowdhury, J. R. Lakowicz, *Nano Lett.* **2007**, 7, 2101.
- [22] F. Gu, L. Zhang, B. A. Teply, N. Mann, A. Wang, A. F. Radovic-Moreno, R. Langer, O. C. Farokhzad, *Proc. Natl. Acad. Sci.* **2008**, 105, 2586.
- [23] H. Park, N. Heldman, P. Rebentrost, L. Abbondanza, A. Iagatti, A. Alessi, B. Patrizi, M. Salvalaggio, L. Bussotti, M. Mohseni, F. Caruso, H. C. Johnsen, R. Fusco, P. Foggi, P. F. Scudo, S. Lloyd, A. M. Belcher, *Nat. Mater.* **2016**, 15, 211.
- [24] J. Xie, C. Xu, N. Kohler, Y. Hou, S. Sun, *Adv. Mater.* **2007**, 19, 3163.
- [25] C. Deeb, X. Zhou, J. Plain, G. P. Wiederrecht, R. Bachelot, M. Russell, P. K. Jain, *J. Phys. Chem. C* **2013**, 117, 10669.

- [26] O. L. Muskens, V. Giannini, J. A. Sánchez-Gil, J. Gómez Rivas, *Nano Lett.* **2007**, *7*, 2871.
- [27] R. I. Nooney, C. M. N. McCahey, O. Stranik, X. Le Guevel, C. McDonagh, B. D. MacCraith, *Anal. Bioanal. Chem.* **2009**, *393*, 1143.
- [28] F. Nicoli, M. K. Roos, E. A. Hemmig, M. Di Antonio, R. de Vivie-Riedle, T. Liedl, *J. Phys. Chem. A* **2016**, *120*, 9941.
- [29] I. Renge, U. P. Wild, *J. Phys. Chem. A* **1997**, *101*, 7977.
- [30] E. Herz, T. Marchincin, L. Connelly, D. Bonner, A. Burns, S. Switalski, U. Wiesner, *J. Fluoresc.* **2010**, *20*, 67.
- [31] J. R. Lakowicz, Y. Shen, S. D'Auria, J. Malicka, J. Fang, Z. Gryczynski, I. Gryczynski, *Anal. Biochem.* **2002**, *301*, 261.



**Scheme 1.** Illustration the synthesis procedure of E3-Cy3-CTPEG-AgNPs complex.

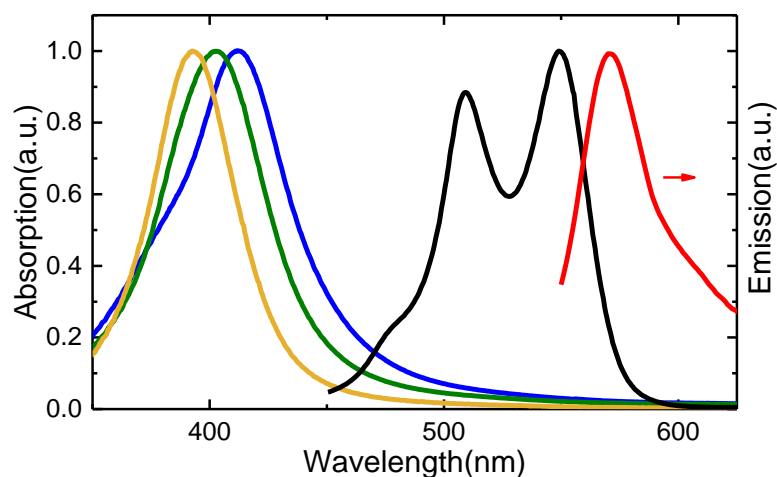


**Figure 1.** Normalized extinction spectrum of AgNPs with diameters of 20 nm (orange line), 30 nm (green line), and 40 nm (blue line), normalized absorption spectrum of E3-Cy3 complex (black line), normalized emission spectrum of E3-Cy3 complex (red line).

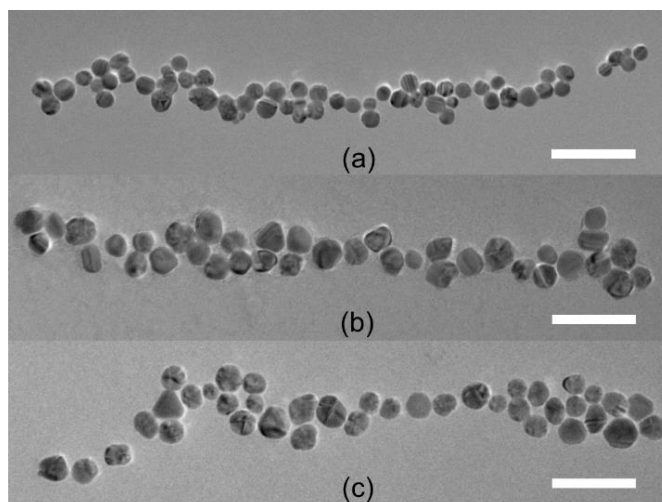
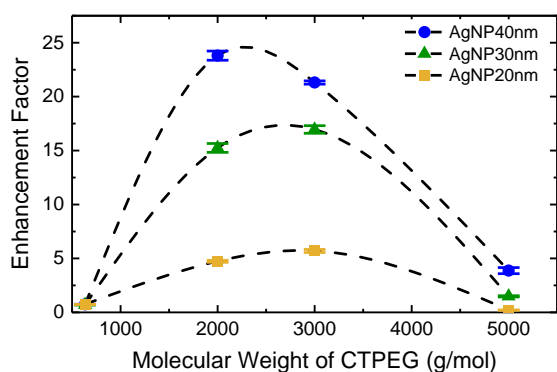
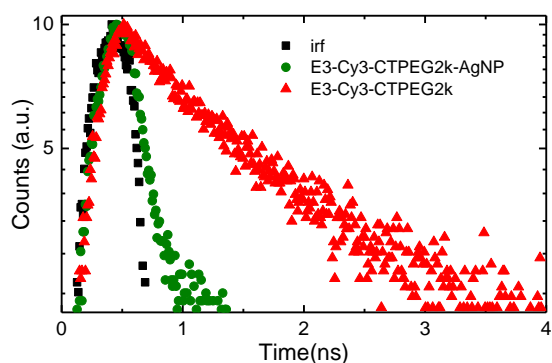


**Figure 2.** Transmission electron micrographs of AgNPs of a) 20 nm b) 30 nm c) 40 nm diameter assembled along the E3 virus surface, which is modified by CTPEG2k molecules. Scale bar is 100 nm.

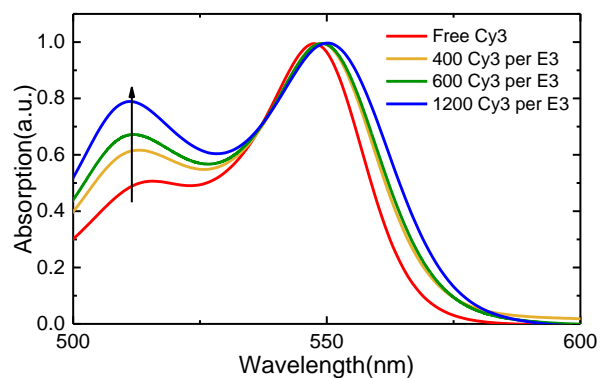


(a)

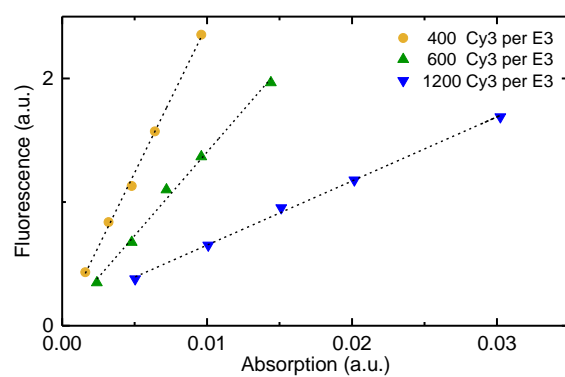


(b)

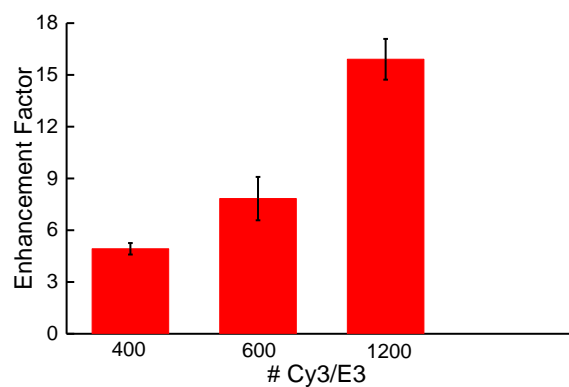
**Figure 3.** a) Fluorescence enhancement factors at different PEG mol.wt. and AgNP sizes (orange square: 20 nm; green triangle: 30 nm; and blue dot: 40 nm). b) Lifetime measurement of E3-Cy3-CTPEG2k (red triangle) and E3-Cy3-CTPEG2k-AgNP30nm (green dot).



(a)



(b)



(c)

**Figure 4.** a) Normalized absorption peaks as function of Cy3 surface density on E3 surface, black arrow indicating the increased hypsochromic peak. b) Illustration of quantum yield measurements of Cy3 dyes of various surface densities. c) Enhancement factor as function of Cy3 surface density with AgNP30nm.

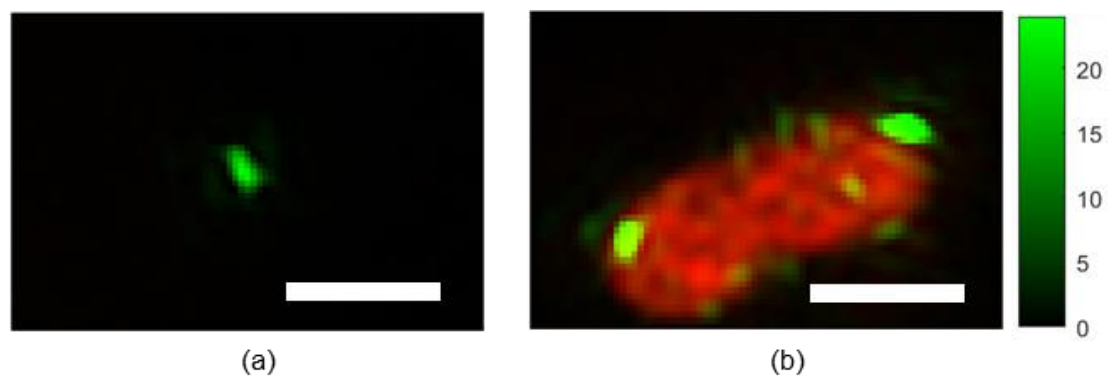


**Figure 5.** Super-resolution fluorescence images of a) E3-CTPEG2k-Cy3-AgNP30nm complex (green). b) *E. coli* stained with Alexa Fluor 647 (red) imaged with E3-CTPEG2k-Cy3-Ag30nm fluorescent probes (green). Scale bar is 1 μm. Color bar is the same for (a) and (b).

## Supporting Information

### **M13 Virus-based Framework for High Fluorescence Enhancement**

*Shengnan Huang, Jifa Qi, Dane W. deQuilettes, Mantao Huang, Ching-Wei Lin, Neelkanth M. Bardhan, Xiangnan Dang, Vladimir Bulović, Angela M. Belcher\**

#### **1. Experiment**

##### **1.1. Synthesis of M13-Cy3-PEG-AgNP Complex**

Cyanine 3 dye and silver nanoparticles were co-assembled on M13 virus surface with carboxy-PEG-thiol (CTPEG) molecules as the spacer. Scheme 1 presents the synthesis of M13-dye-silver nanoparticle nanocomposite. Organic dye molecules of sulfo-Cy3-NHS ester (Lumiprobe, MD, USA, Cy3) were conjugated to the exposed amine groups with the formation of amide bond. The typical synthesis procedure of the nanocomplex is described here for reference. Specifically, 36  $\mu\text{L}$  of 30 mM sulfo-Cy3-NHS ester in anhydrous dimethyl sulfoxide (DMSO) was added into 180  $\mu\text{L}$  E3 virus (one clone of M13 virus, with the EEE oligomer insert into the p8 sequence, was chosen for its easy amplification) with concentration of  $3.4 \times 10^{13}/\text{mL}$  in PBS 1 $\times$  (pH  $\sim 7.4$ ) and reacted overnight. Excess dye molecules were removed by extensive dialysis in dark using a 100 kDa cutoff membrane (Spectrum Laboratories, CA, USA) against PBS 1 $\times$  buffer for 2 days. The absorption spectrum of E3 conjugated with Cy3 (henceforth referred to as the E3-Cy3 complex) was then measured with DU800 (Beckman Coulter).

After Cy3 dye was conjugated to E3 surface, the next step was to conjugate CTPEG molecules to the E3 surface. The carboxylic group of CTPEG (100 mM) was first activated by using (1-ethyl-3-(3 dimethylaminopropyl) carbodiimide hydrochloride) (200 mM) (EDC, Thermo Fisher Scientific, PA, USA) and N-Hydroxysuccinimide (200 mM) (NHS, Aldrich, MO, USA) in anhydrous DMSO. The molar ratio between CTPEG, EDC, and NHS was kept to be 1:1:1. Then 2.1  $\mu\text{L}$  of the activated CTPEG molecules with concentration of 50 mM (of varying molecular weights, namely, 635, 2000, 3000 and 5000 g/mol) was reacted with 20  $\mu\text{L}$  of the E3-Cy3 complex ( $2.9 \times 10^{13}/\text{mL}$ ) in PBS 1 $\times$  overnight. Free CTPEG molecules were removed by dialysis



in dark using 100 kDa cutoff membrane against PBS 1× buffer for 2 days. By this step, E3-Cy3-CTPEG complex was formed.

For the nanocomplex synthesis in Figure 4, 200  $\mu\text{L}$  of E3 virus ( $3 \times 10^{13}/\text{mL}$ ) in PBS 1 × was first conjugated with 21.5  $\mu\text{L}$  of activated CTPEGs (50mM) in DMSO. The free CTPEG molecules were removed by extensive dialysis using a 100 kDa cutoff membrane. Then 3.2  $\mu\text{L}$ , 1.6  $\mu\text{L}$  and 0.5  $\mu\text{L}$  of Cy3 (30mM) was added to 20  $\mu\text{L}$  of E3-CTPEG complex ( $2.7 \times 10^{13}/\text{mL}$ ) to synthesize E3-CTPEG-Cy3 complex with different dye surface densities. The free Cy3 molecules were removed by extensive dialysis in dark using a 100 kDa cutoff membrane. The reaction ratio between free amines exposed on the M13 virus surface and the activated CTPEG molecules is 1:20 (meaning 20 × excess of the SH-PEG-NHS molecules) for both Figure 3 and Figure 4. This ratio is chosen to maximize the number of PEG molecules conjugated to the virus surface.

Citrate capped spherical silver nanoparticles (AgNPs) with diameter of 20 nm, 30 nm and 40 nm were purchased from Nanocomposix (CA, USA). AgNPs were attached to the exposed thiol groups of the PEG molecules in the E3-Cy3-CTPEG or E3-CTPEG-Cy3 complex (hereafter, denoted as E3-Cy3-CTPEG-AgNP / E3-CTPEG-Cy3-AgNP complex). The reaction ratio between AgNPs of various diameters and E3-Cy3-CTPEG of various CTPEG molecular weights is summarized below in Table S1,

**Table S1.** Reaction ratios between AgNPs of various size and E3-Cy3-CTPEG of various CTPEG molecular weights

AgNP size(nm)	virus:AgNP ratio(number ratio)	$[AgNP]_0^*$ (#/mL)	$[virus]_0^*$ (#/mL)	$[virus]_f^\#$ (#/mL)
20	1:50	$5.2 \times 10^{11}$	$1.5 \times 10^{10}$	$6.2 \times 10^9$
30	1:35	$1.1 \times 10^{11}$	$1.5 \times 10^{10}$	$2.6 \times 10^9$
40	1:25	$1.1 \times 10^{11}$	$1.5 \times 10^{10}$	$2.1 \times 10^9$

\*: initial concentration of AgNP and M13 virus before mixing of AgNP and M13 virus

#: final concentration of M13 virus after mixing of AgNP and M13 virus

## 1.2. TEM, Fluorescence and Lifetime Measurement

The transmission electron microscope (TEM) image of the E3-Cy3-CTPEG-AgNP complex was taken using JEOL 2010 Advanced High Performance TEM.

The fluorescence spectrum was measured on a NanoLog spectrofluorometer (Horiba Jobin Yvon Inc.) with 1 cm path-length quartz cuvette. In the spectrofluorometer, a laser diode of CPS 532 (Thor Labs) was used as the excitation source (continue wave, average power 5mW). The fluorescence signal was detected by a single photon counting multiplier at a working voltage of 950V.

Optical spectroscopy was performed using a Nikon Eclipse-Ti inverted microscope fitted with an infinity corrected 10 × dry objective (Nikon Plan Fluor, NA = 0.3). The excitation wavelength was set at 510 nm by wavelength selecting the broadband emission from a supercontinuum laser (NKT Photonics SuperK Extreme, 40 MHz, 500 nJ cm<sup>-2</sup> per pulse) sent through an acousto-optic modulator (NKT Photonics Supertrek dual, ~3 nm bandwidth) driven by a radio-frequency function generator (Stanford Research Instruments, Inc. Model SG382) and amplifier at a frequency of 125.9 MHz. The laser output beam was sent through a 550 nm shortpass filter before photoexcitation and the sample emission was filtered through a 532 nm laser BrightLine single-edge laser-flat dichroic beamsplitter (Semrock DiO2-R532) as well as an additional 550 nm long pass filter then coupled in free space into a streak camera (Hamamatsu C5680) equipped with a slow speed sweep unit (M5677). The time delay between the laser source and sweep unit was controlled using a digital delay generator (Stanford Research Systems, Inc. Model DG645). Data was collected using the time-correlated single photon counting mode in the HPD-TA 8.4.0 software (Hamamatsu).

## 2. Fluorescence Enhancement of AgNPs vs. AuNPs

### 2.1. Theoretical Calculation of the Spectral Dependence of Enhancement Factor<sup>[1,2]</sup>

The fluorescence enhancement factor (EF, or  $\gamma_{em}/\gamma_{em}^0$ ) is the product of the excitation rate enhancement ( $\gamma_{exc}/\gamma_{exc}^0$ ) and the modified quantum yield ratio ( $q/q^0$ ), which can be written as follows:

$$EF = \frac{\gamma_{em}}{\gamma_{em}^0} = \frac{\gamma_{exc}}{\gamma_{exc}^0} \frac{q}{q^0} \quad (S1)$$

where  $\gamma_{em}$ ,  $\gamma_{exc}$  and  $q$  are the enhanced emission rate, the excitation rate and the quantum yield of fluorophores in the presence of metal nanoparticles, respectively.  $\gamma_{em}^0$ ,  $\gamma_{exc}^0$  and  $q^0$  are the intrinsic emission rate, intrinsic excitation rate and intrinsic quantum yield of fluorophores in free space, respectively. The excitation rate enhancement ( $\gamma_{exc}/\gamma_{exc}^0$ ) can be expressed as follows, assuming spherical plasmonic nanoparticles are used:

$$\frac{\gamma_{exc}}{\gamma_{exc}^0} = \left| 1 + \frac{2a^3}{(a+z)^3} \frac{\varepsilon(\omega_1)-1}{\varepsilon(\omega_1)+2} \right|^2 \quad (S2)$$

where  $\varepsilon(\omega_1)$  is the wavelength-dependent dielectric constant of the nanoparticle,  $\omega_1$  is the excitation frequency,  $a$  is the radius of the spherical nanoparticle,  $z$  is the fluorophore-metal nanoparticle edge distance. The quantum yield enhancement can be expressed as:

$$\frac{q}{q^0} = \frac{1}{q^0} \frac{\gamma_r/\gamma_r^0}{\gamma_r/\gamma_r^0 + \gamma_{abs}/\gamma_r^0 + (1-q^0)/q^0} \quad (S3)$$

where  $\gamma_r/\gamma_r^0$  is the radiative rate enhancement ( $\gamma_r$  is the enhanced radiative decay rate,  $\gamma_r^0$  is the radiative decay rate of fluorophores in free space) as shown in Equation 4.

$$\frac{\gamma_r}{\gamma_r^0} = \left| 1 + \frac{2a^3}{(a+z)^3} \frac{\varepsilon(\omega_2)-1}{\varepsilon(\omega_2)+2} \right|^2 \quad (S4)$$

where  $\varepsilon(\omega_2)$  is the wavelength dependent dielectric constant of nanoparticle,  $\omega_2$  is the emission frequency.  $\gamma_{abs}/\gamma_r^0$  is the nonradiative decay rate increases due to dissipative energy transfer from fluorophore to metal nanoparticle, which can be expressed as:

$$\frac{\gamma_{abs}}{\gamma_r^0} \approx \frac{3}{8} \text{Im} \frac{\varepsilon(\omega_2)-1}{\varepsilon(\omega_2)+1} \frac{1}{(k_2 z)^3} \quad (S5)$$

where  $k_2$  is the wavenumber of the emission.

Combining Equations S1-5, the spectral dependence of fluorescence EF can be deduced.

The spectral dependence of excitation rate enhancement and quantum yield enhancement by AgNP40nm is shown in Figure S1a, c accordingly (blue line). The excitation rate enhancement and quantum yield enhancement both increase when approaching the plasmon resonance peak of AgNP40nm (~ 400 nm). As a result, the EF of AgNP40nm increases with the excitation and emission wavelength when approaching the plasmon resonance peak of AgNP40nm (~400 nm)

as shown in Figure S1b. Figure S1b is plotted by expanding the plot by Bharadwaj et al.<sup>[1]</sup> For our case, when the absorption of the M13-Cy3 complex is 500~550 nm and emission peak is 570 nm, the excitation rate is enhanced by ~7 fold and the quantum yield is enhanced by ~3.5 fold, producing a ~ 24-fold fluorescence enhancement by utilizing AgNP40nm. Hence, even though the absorption/emission spectra of M13-Cy3 complex are red-shifted compared to the plasmon resonance of AgNP and there is small overlap between them, the M13-Cy3 is able to interact with the plasmons of AgNP to gain fluorescence enhancement. It has been reported that AgNP was used to enhance the emission of Cy5 dye with excitation wavelength of 635 nm and emission wavelength of 655 nm<sup>[3]</sup>.

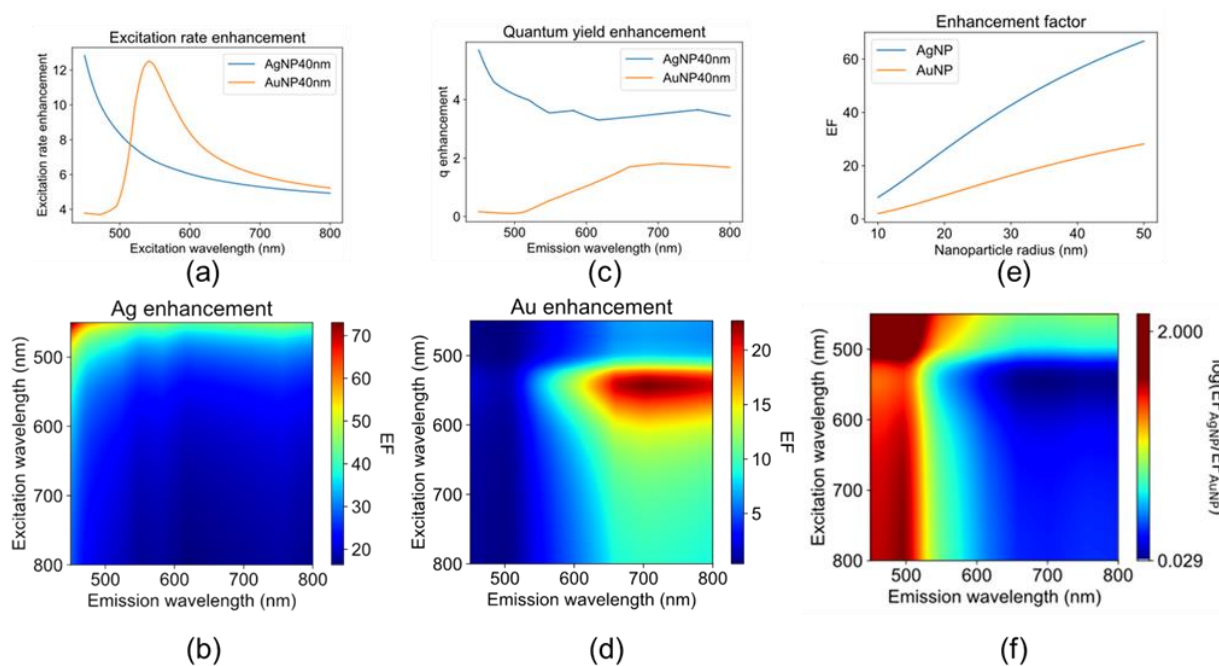


**Figure S1.** (a) Excitation rate enhancement of AgNP40nm (blue) and AuNP40nm (orange) as function of the excitation wavelength. (b) EF spectral dependence of AgNP40nm. (c) Quantum yield enhancement of AgNP40nm (blue) and AuNP40nm (orange) as function of emission wavelength. (d) EF spectral dependence of AuNP40nm. (e) EF as function of AgNP (blue) and AuNP (orange) size. (f) Spectral dependence of ratio of EF of AgNP40nm ( $EF_{AgNP}$ ) over EF of AuNP40nm ( $EF_{AuNP}$ ) in log scale. The minimum value of the scale bar is 0.029. The calculation parameters for (a-d,f) are:  $\alpha_{AgNP} = \alpha_{AuNP} = 20$  nm,  $q^0 = 0.03$ ,  $z = 5$  nm. The calculation parameters for (f) are: excitation wavelength = 532 nm, emission wavelength = 570 nm,  $q^0 = 0.03$ ,  $z = 5$  nm.

## 2.2. Materials Selection AgNP vs. AuNP

Another candidate for achieving fluorescence enhancement is gold nanoparticles (AuNP) which have plasmon resonance of ~ 520 nm, overlapping more with the absorption/emission of M13-Cy3 complex compared to AgNP (Figure S2b). However, both theoretical calculations (Figure

S1d-f) and experiment results (Figure S2d) show that AuNP gives much smaller fluorescence enhancement than AgNP for a given size and metal-fluorophore distance. Note in Figure S1f, the scale bar is in log scale with a minimum value 0.029, indicating that the EF of AgNP is larger than that of AuNP across all the excitation/emission wavelengths in Figure 1f. For our M13-Cy3 complex, although AuNP40nm offers similar excitation rate enhancement as AgNP40nm (Figure S1a) at excitation wavelength of 532 nm, the quantum yield enhancement for AuNP40nm is much smaller (quenching) compared to AgNP40nm (Figure S1b) because of the strong AuNP dissipative energy transfer. On the contrary, AgNP40nm offers a strong quantum yield enhancement. Overall, AgNP40 nm gives much higher EF than AuNP40nm for our M13-Cy3 complex.

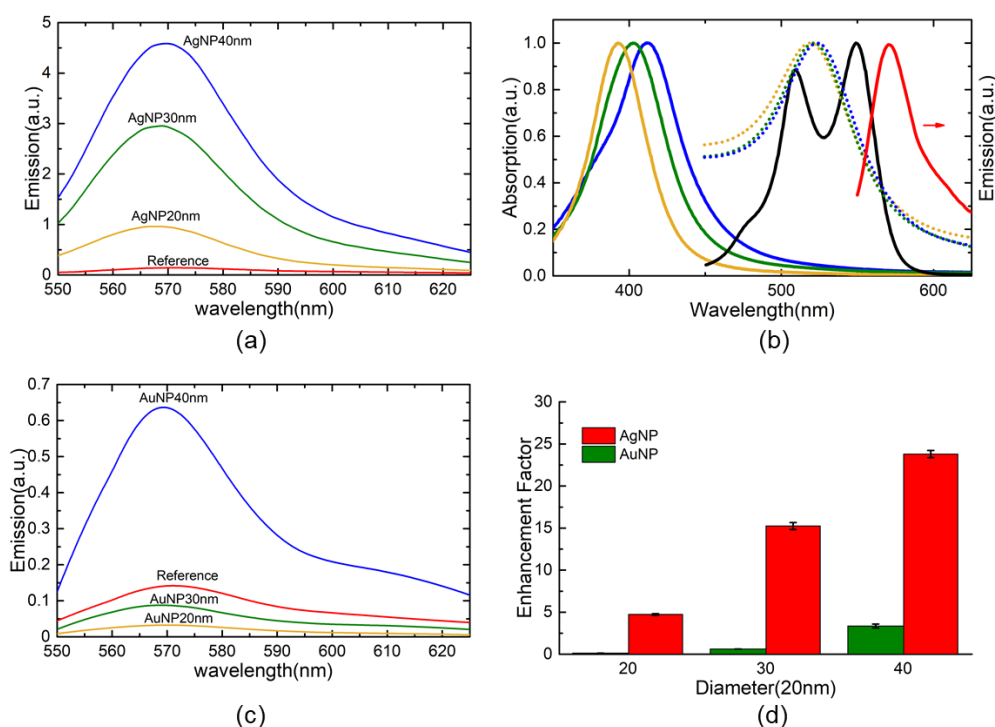


**Figure S2.** (a) Emission spectrum of E3-Cy3-CTPEG2k-AgNP20/30/40 nm. (b) Extinction spectrum of AgNPs of 20 nm (orange line), 30 nm (green line), and 40 nm (blue line) and AuNPs of 20 nm (dotted orange line), 30nm (dotted green line) and 40 nm (dotted blue line); absorption spectrum of E3-Cy3 complex (black line); emission spectrum of E3-Cy3 complex (red). (c) Emission spectrum of E3-Cy3-CTPEG2k-AuNP20/30/40nm. (d) Experimental fluorescence enhancement factor of AuNP (green) and AgNP (red) with diameter of 20/30/40 nm.

### 2.3. Constraint of M13 Template

Theoretical calculations (Figure S1e) shows that AuNP with a size of 100 nm is able to give us similar enhancement factor as AgNP with a size of 40 nm for M13-Cy3. However, our M13 phage template is suitable for assembling small nanoparticles due to its geometrical constraint. In addition, nanoparticles with diameters larger than 100 nm lead to *in vivo* circulation and clearance problems. Hence, AgNP with smaller sizes is desirable.

In summary, although the absorption (~500-550 nm) and emission (peak at 570 nm) spectrum of M13-Cy3 complex is redshifted compared to the plasmon resonance peak of AgNP40nm (~400 nm), the M13-Cy3 is able to interact with the plasmon of AgNPs to gain fluorescence enhancement through excitation rate enhancement and quantum yield enhancement. On the contrary, AuNP40nm, whose plasmon resonance overlaps more with the absorption/emission spectrum of M13-Cy3, quenches the quantum yield of M13-Cy3 and offers a much smaller overall EF than AgNP40nm. Even though bigger AuNPs are able to achieve similar EF as smaller AgNPs. The nanoparticle size is actually more important for practical applications. Hence, AgNPs are better choices than AuNPs because their enhancements are stronger at smaller size.

### 3. Low Magnification TEM Images of E3-CTPEG2k-AgNPs

The assembly of metal nanoparticles on virus surface and the agglomeration occurrence are related to the experimental conditions. In the reaction mixture of virus and AgNPs, the number ratios between M13 virus and AgNPs are chosen (see Table S1) to enable enough virus surface interacting with the nanoparticles and most of the nanoparticles would bind to the virus surface. Furthermore, the concentration of virus is controlled to be very low (on the order of  $10^9$ /mL, Table S2) to avoid the agglomeration of probes. In a well-controlled situation, most of the particles are correctly assembled as shown in Figure S3 in this reply.

As shown in the low magnification TEM images of the E3-CTPEG2k-AgNP20nm/30nm/40nm in Figure S3, very few free AgNPs are observed. It can be considered that most of the metal nanoparticles are assembled on the surface of virus. There is minor agglomeration of the probes as evidenced by the low magnification TEM images. The agglomeration might be induced in the TEM sample preparation process. Under our normal TEM sample preparation process, the sample was diluted so that we are able to find isolated probes in the TEM field of view and the typical images of single probes were provided in the manuscript main text. However, in order to have multiple viruses under the field of view, we use higher concentration of probes for TEM sample preparation; this may cause the overlap or agglomeration of the probes.

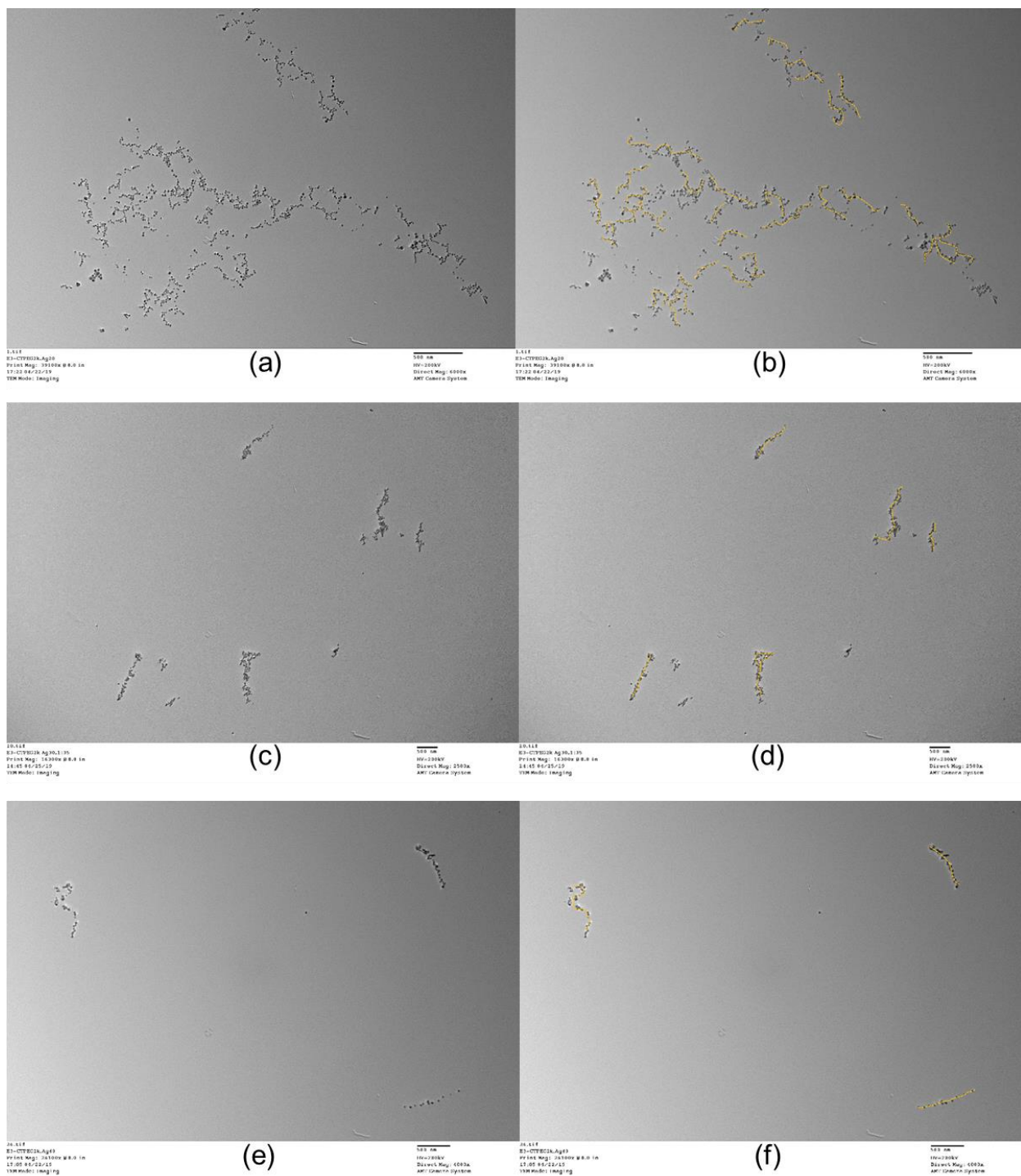


**Figure S3.** Low magnification TEM image of E3-CTPEG2k-(a) AgNP20nm (c) 30nm (e) 40nm. Using orange dotted lines to indicate the M13 virus of E3-CTPEG2k-(b) AgNP20 nm (d) 30nm (f) 40nm. Scale bar is 500 nm.



### 3. Absorption Spectrum of E3-Cy3-CTPEG-AgNPs

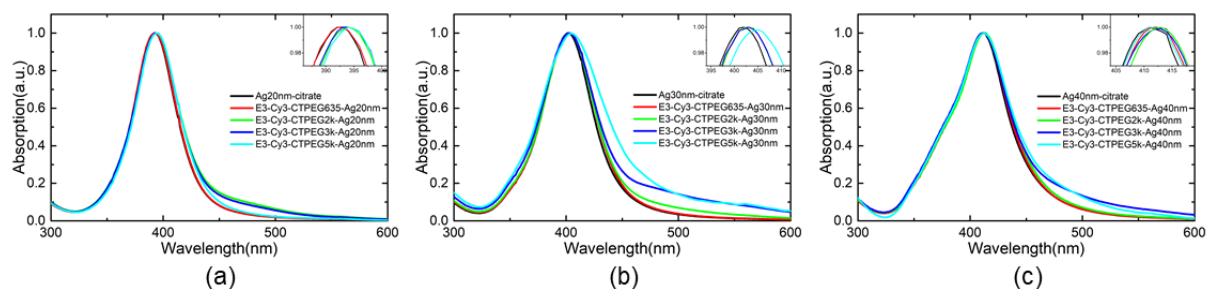


**Figure S4.** Absorption spectrum of E3-Cy3-CTPEG-AgNP for different sizes of the Ag nanoparticles:(a) 20 nm, (b) 30 nm, (c) 40 nm, inset showing the peak shift after complexing.

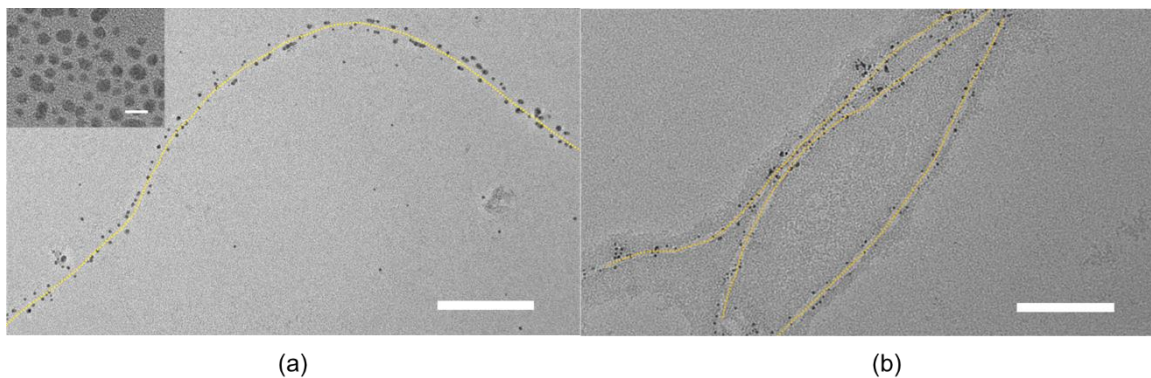
### 4. Surface Density of Cy3 in Figure 3

**Table S2.** Calculation of surface grafting density of Cy3 on E3 surface in Figure 3

[E3]/mL	$2.87 \times 10^{13}$
OD @ maximum	15.4
Extinction Coefficient ((Mcm) <sup>-1</sup> )	162000
[Cy3]/ $\mu$ M	95.06
#Cy3/E3	1990

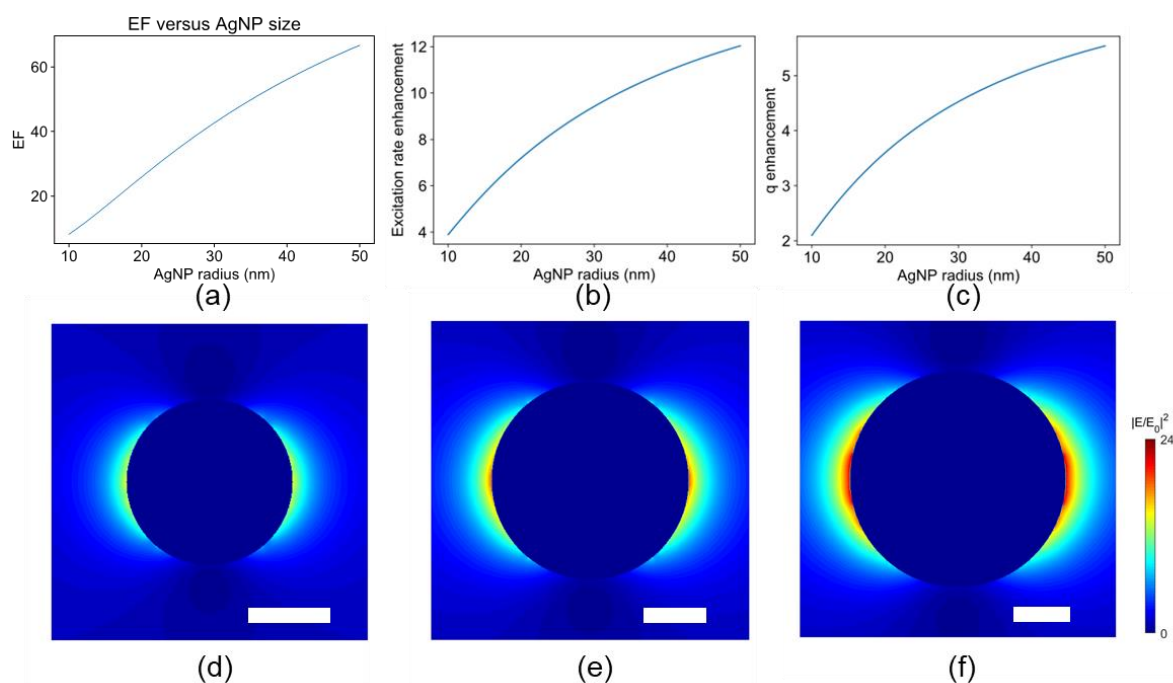
### 5. Cy3-AgNP Distance Control with CTPEGs

Figure S5 shows M13 virus modified with CTPEG molecules and stained with AuNPs with diameter of 2 ~3 nm (inset of Figure S5a). The PEG spacer thickness can be found by measuring the distance between gold nanoparticles on the two sides of the M13 virus (excluding the diameter of M13 virus of 6.5 nm). The spacer thickness for E3-Cy3-CTPEG3k in Figure S5a is measured to be ~ 6 nm. This is consistent with the literature that fluorescent enhancement occurs when fluorophore-metal nanoparticle distance is within 10 nm.<sup>[2,4]</sup> For the case of CTPEG with molecular weight of 635 g/mol shown Figure S5b, the spacer provided is around 3 nm. This small thickness results in small enhancement as shown in Figure 3a of the manuscript main text.



**Figure S5.** TEM images of small gold nanoparticles stained (a) E3-Cy3-CTPEG3k and (b) E3-Cy3-CTPEG635 nanocomplex. Orange dotted line indicates E3 virus. Scale bar is 100 nm in (a) and (b). In (b), the E3 virus is stained with uranyl acetate. Inset in (a) shows the TEM image of the gold nanocolloids for staining. Scale bar is 5 nm.

## 6. AgNP Size Effect on Fluorescence Enhancement



**Figure S6.** (a) Enhancement factor (b)Excitation rate enhancement and (c) Quantum yield enhancement as function of AgNP radius for M13-Cy3 complex. Calculation conditions:  $q^0 = 0.03$ ,  $z = 5$  nm, excitation wavelength=532 nm, emission wavelength=570 nm . FDTD simulation of the electric field distribution@532 nm for AgNP of (d) 20 nm (e)30 nm and (f)40 nm. Scale bar is 10 nm.

Larger fluorescence enhancement is expected with larger AgNP as shown in Figure S6 (a). With increasing nanoparticle size, the local electric field enhancement is increased(Figure S6 d-f) resulting in stronger excitation rate enhancement (Figure S6 (b)). As the effect of nanoparticle size on nonradiative decay rate is less effective with larger nanoparticles<sup>[5]</sup> and the radiative

decays rate increases with nanoparticle size, the quantum yield enhancement also increases with nanoparticle size (Figure S6(c)). Hence, larger enhancement is expected with bigger AgNPs.

## 7. Cy3 Surface Density Calculation

Figure S7 shows the absorption spectrum of E3 virus conjugated with Cy3 of various surface densities. The number of copies of Cy3 dyes per E3 virus is calculated using Beer-Lambert law, assuming the extinction coefficient of free Cy3 and Cy3 conjugated to E3 virus surface is the same. The results are summarized in Table S3.

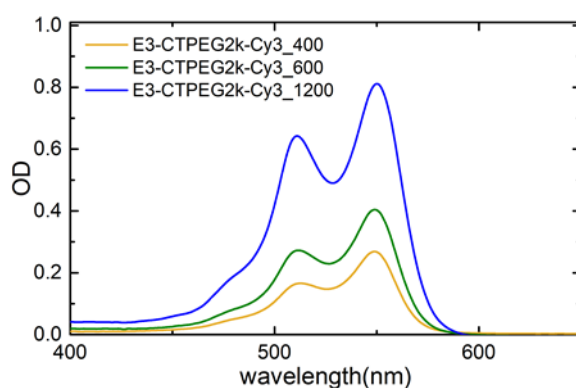


**Figure S7.** Absorption spectrum of E3 conjugated with various Cy3 surface densities. The complex is named is such a manner as E3-CTPEG2k-Cy3\_#dye per virus.

**Table S3.** Calculation of Cy3 surface density on E3 virus

	E3-CTPEG2k-Cy3_400	E3-CTPEG2k-Cy3_600	E3-CTPEG2k-Cy3_1200
OD @ maximum	0.27	0.405	0.812
Extinction Coefficient ( $Mcm$ ) <sup>-1</sup>	162000	162000	162000
[Cy3]/uM	2.08	3.12	6.27
[E3]/mL	$2.5 \times 10^{12}$	$2.5 \times 10^{12}$	$2.5 \times 10^{12}$
#Cy3/E3	~400	~600	~1200

## 8. Intrinsic Quantum Yield Effect on Fluorescence Enhancement

Upon placing metal nanoparticle near fluorophore, there will be enhanced radiative decay rate ( $\gamma_r$ ) and new non-radiative decay rate ( $\gamma_{rabs}$ ), both of which are independent of the fluorophore. The effect of this is to bring the modified quantum yield ( $q$ ) of the fluorophore close to the

value of  $\frac{\gamma_r}{\gamma_r + \gamma_{rabs}}$ . This effect is more prominent when the fluorophore has lower intrinsic quantum yield ( $q^0$ ). Hence, fluorophores with lower quantum yield will have higher quantum yield enhancement ( $\frac{q}{q^0}$ ) and higher fluorescence enhancement. For our case, when increasing the dye density, the quantum yield of Cy3 is lowered due to intermolecular quenching. Hence, higher EF is expected at higher Cy3 density.

The details of the above are explained below with equations and plots:

$$q = \frac{\gamma_r}{\gamma_r + \gamma_{abs} + \gamma_{nr}^0} = \frac{\gamma_r / \gamma_r^0}{\gamma_r / \gamma_r^0 + \gamma_{abs} / \gamma_r^0 + (1 - q^0) / q^0} \quad (S6)$$

$$EF = \frac{\gamma_{exc}}{\gamma_{exc}^0} \frac{q}{q^0} = \frac{\gamma_{exc}}{\gamma_{exc}^0} \frac{1}{q^0} \frac{\gamma_r / \gamma_r^0}{\gamma_r / \gamma_r^0 + \gamma_{abs} / \gamma_r^0 + (1 - q^0) / q^0} \quad (S7)$$

where  $\gamma_r^0$  and  $\gamma_{nr}^0$  are the intrinsic radiative decay rate and intrinsic nonradiative rate of the fluorophore.

Let  $m = \gamma_{exc} / \gamma_{exc}^0 = \gamma_r / \gamma_r^0$  (assuming Stokes shift is small) and  $n = \gamma_{abs} / \gamma_r$

$$EF = \frac{m^2}{q^0(m + n - 1) + 1}$$

$$\frac{q}{q^0} = \frac{m}{q^0(m + n - 1) + 1}$$

where m and n are independent of intrinsic fluorophore quantum yield  $q^0$ . Applying the same parameters into the formula, the enhancement factor and quantum yield enhancement with respect to the intrinsic quantum yield are shown in Figure S8 (a) and (b),

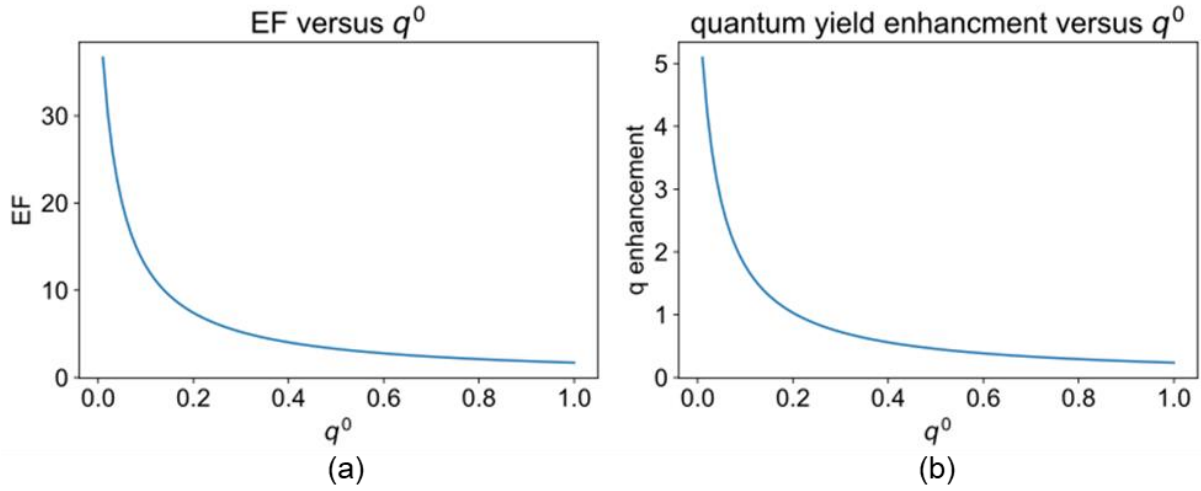


**Figure S8.** (a) Enhancement factor as function of the intrinsic quantum yield  $q^0$ , (b) Quantum yield enhancement as function of  $q^0$ . The calculation conditions:  $a_{AgNP} = 20nm$ ,  $z = 5nm$ , excitation wavelength=532 nm, emission wavelength=570 nm

## 9. Calculation of Fluorescence Enhancement Factor

The enhancement factor was calculated by comparing the integrated fluorescence intensity of E3-Cy3-CTPEG-AgNP samples (after subtracting the dark current) to that of E3-Cy3-CTPEG (after subtracting the dark current), as shown in Equation S8. The concentration (or Optical Density, O.D.) of E3-Cy3-CTPEG is kept constant for comparing E3-Cy3-CTPEG-AgNPs samples and E3-Cy3-CTPEG reference samples.

$$EF = \frac{I_X - I_{dark\ current}}{I_{reference} - I_{dark\ current}} \quad (S8)$$

where  $I_X$  is the integrated fluorescence intensity of sample X (X stands for E3-Cy3-CTPEG-AgNP complex),  $I_{reference}$  is the integrated fluorescence intensity of the reference sample (E3-Cy3-CTPEG) and  $I_{dark\ current}$  is the integrated fluorescence intensity of the dark current.

## 10. Fluorescence Probe binding with *E. coli* and Super-resolution Microscope

*E.coli* cells were first stained with Alexa Fluor 647 by mixing the cells with Alexa Fluor 647-NHS ester in growth medium at 37 degree in 5% CO<sub>2</sub> incubator for 4 hours and *E. coli* cells were spin down and re-disperse in growth medium. Next, the Alexa Fluor 647 stained *E.coli* cells were mixed with E3-Cy3-CPEG2k and E3-Cy3-CPEG2k probes (with 1000 probes per *E. coli* for both cases) separately overnight in the incubator. Then the above *E. coli* cells were

mixed with appropriate amount of mounting medium and around 10uL was placed on glass slide and then covered by glass cover slip.

*E. coli* cells were imaged with a GE Delta-OMX V4 Blaze 3D structured illumination microscope, equipped with 405 nm, 488 nm, 563 nm and 647 nm lasers and three sCMOS cameras. Images were acquired with a 60X, NA 1.43 oil objective, at 0.125 micron z step, using 1.518 immersion oil, at RT. All images were acquired under the same illumination settings and then processed with OMX softWoRx software (Applied Precision/GE). Images were saved as tiff.

### 11. *E. coli* Stained with Fluorescent Probes

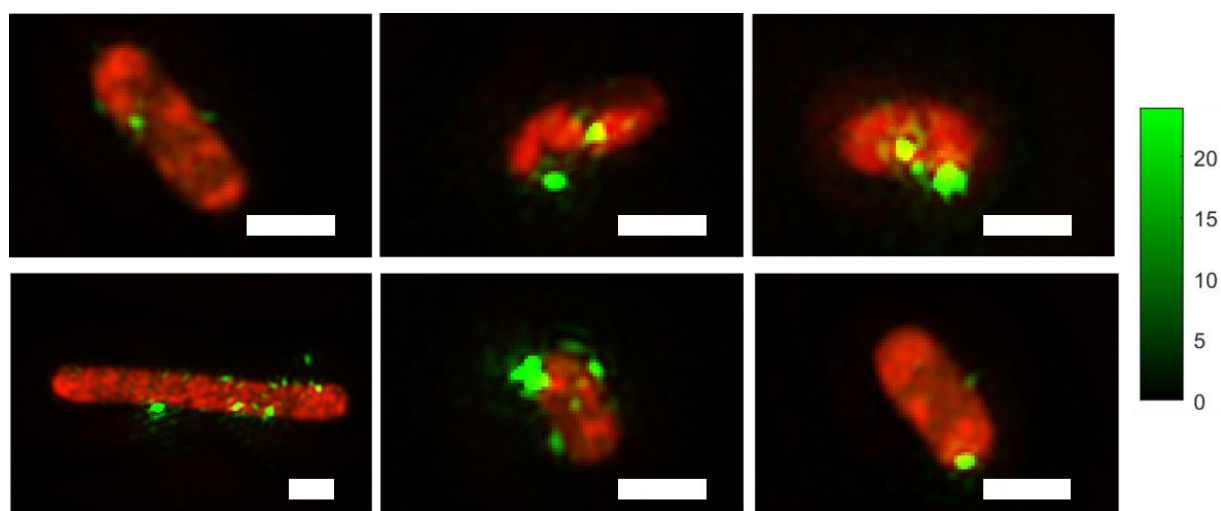


**Figure S9.** Extra examples of *E. coli* stained with surface plasmon enhanced fluorescent probes. Scale bar is 1  $\mu$ m.

### 11. PEG Molecular Weight at Maximum EF

Based on our calculation, the Cy3-AgNP distance at maximum EF increases with the AgNP size as shown in Figure S10. The change in the distance at maximum EF is less than 1 nm (corresponding to ~100g/mol of linear PEG) when the AgNP size changes from 20 nm to 40 nm. This should lead to EF peaking at similar CTPEG for the AgNPs we studied in Figure 3a. However, it is observed that the EF of larger AgNPs peaks at PEG of lower molecular weight in Figure 3a, which could be possibly due to the following reason:

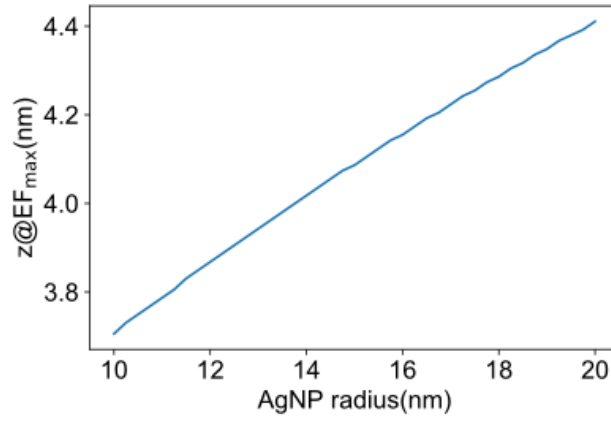


**Figure S10.** The distance at maximum EF vs. AgNP size, calculation conditions: excitation wavelength=532 nm, emission wavelength=570 nm,  $q^0 = 0.03$ .

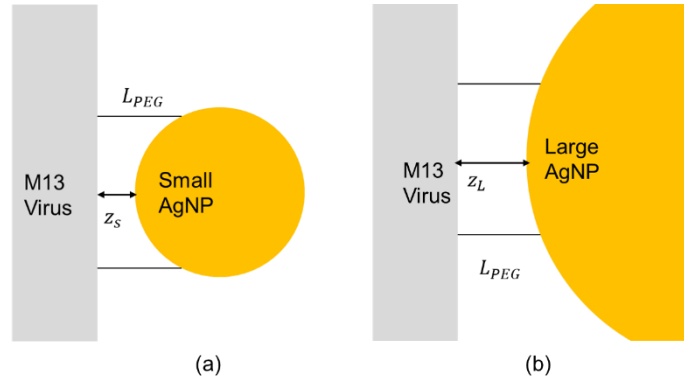


**Figure S11.** Cy3-AgNP distance comparison between (a) small and (b) large AgNP with the same PEG molecular weight.

Assume that PEG molecules in the M13-Cy3-CTPEG complex are in extended form interacting well with the water molecules in solution.<sup>[6]</sup> Upon inclusion of AgNPs to form the M13-Cy3-CTPEG-AgNP complex, the maximum distance from the AgNP surface to the M13 surface is limited by the molecular weight of the PEG as indicated by  $L_{PEG}$  in Figure S11. Hence, for the PEG with the same molecular weight, AgNP with smaller surface curvature (larger size) has larger minimum distance ( $z_L$ ) between the AgNP and M13 than that of AgNP with larger surface curvature (smaller size) as  $z_s$  in Figure S11. That is to say, for the M13-Cy3-CTPEG-AgNP complex with the same PEG, the Cy3-AgNP distance increases with increasing AgNP size. This effect is expected to be small because it is similar to the phenomenon that PEG layer thickness increases slightly with nanoparticle core diameter for PEG of the same molecular weight.<sup>[7]</sup> This may be one of the reasons that contribute to the observation that bigger AgNP

has EF peaking at PEG of smaller molecule weight than smaller AgNPs. However, the exact relationship between PEG molecular weight and M13-Cy3-AgNP distance needs further study.

## References

- [1] P. Bharadwaj, L. Novotny, *Opt. Express* **2007**, *15*, 14266.
- [2] P. Anger, P. Bharadwaj, L. Novotny, *Phys. Rev. Lett.* **2006**, *96*, 3.
- [3] J. Zhang, Y. Fu, M. H. Chowdhury, J. R. Lakowicz, *Nano Lett.* **2007**, *7*, 2101.
- [4] A. L. Feng, M. L. You, L. Tian, S. Singamaneni, M. Liu, Z. Duan, T. J. Lu, F. Xu, M. Lin, *Sci. Rep.* **2015**, *5*, 1.
- [5] S. Vukovic, S. Corni, B. Mennucci, *J. Phys. Chem. C* **2009**, *113*, 121.
- [6] R. Y. H. Lim, J. Deng, *ACS Nano* **2009**, *3*, 2911.
- [7] C. Minelli, A. G. Shard, *Biointerphases* **2016**, *11*, 04B306.